CHEMISTRY OF MATERIALS

ARTICLE

pubs.acs.org/cm

New Quaternary Hydride $CeZnSnH_{1.5}$: Structure, Magnetism, and Chemical Bonding

Wilfried Hermes,[†] Bernard Chevalier,[*,‡] Ute Ch. Rodewald,[†] Samir F. Matar,[‡] François Weill,[‡,§] Inga Schellenberg,[†] Rainer Pöttgen,[*,†] Heiko Lueken,[⊥] and Manfred Speldrich[⊥]

[†]Institut für Anorganische und Analytische Chemie and NRW Graduate School of Chemistry, Universität Münster, Corrensstrasse 30, D-48149 Münster, Germany

[‡]CNRS, Université de Bordeaux, ICMCB, 87 Avenue du Docteur Albert Schweitzer, 33608 Pessac Cedex, France

[§]Université de Bordeaux, CREMEM, 33405 Talence, France

[⊥]Institut für Anorganische Chemie, RWTH Aachen University, Landoltweg 1, D-52056 Aachen, Germany

ABSTRACT: The quaternary hydride $CeZnSnH_{1.5}$ was synthesized from a CeZnSn precursor upon hydrogenation at 553 K and 4 MPa H_2 pressure. Single-crystal X-ray diffraction data reveal that the metal atoms adopt an YPtAs-type structure: $P6_3/mmc$, $a = 449.34(9)$ and $c = 1731.3(4)$ pm, w$R2 = 0.0493$, 218 F^2 values, and 12 variables. The hydrogen atoms fill three crystallographically independent $ZnCe_3$ tetrahedral sites, leading to the composition $CeZnSnH_{1.5}$. Hydrogenation anisotropically modifies the unit cell parameters, i.e., 456.7 → 449.34 pm (−1.6%) for a and 1673.8 → 1731.3 pm (+3.4%) for c. This leads to a drastic flattening of the two-dimensional [ZnSn] layers and a decrease of the Zn−Sn distances from 271 to 260 pm. Hydrogenation increases the Curie temperature from 4.8 K for CeZnSn to 7.3 K for $CeZnSnH_{1.5}$.

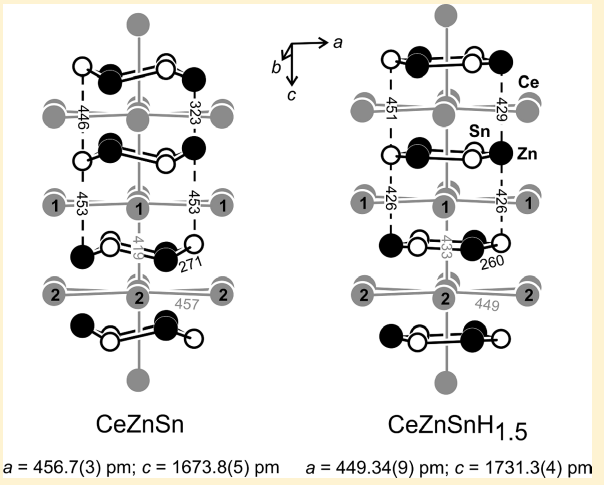

KEYWORDS: hydride, crystal chemistry, $CeZnSnH_{1.5}$, magnetic properties, electronic structure

INTRODUCTION

The equiatomic intermetallic cerium compounds Ce*TX* (*T* = late transition metal; *X* = element of the third, fourth, or fifth main group) show a variety of highly interesting physical properties such as antiferro- or ferromagnetic ordering, spin-fluctuation behavior, static or dynamic intermediate cerium valence, Kondo behavior, or superconductivity. Overviews on the literature are given in refs 1 and 2. The magnetic and transport properties of these intermetallics strongly depend on the hybridization between the 4f(Ce) electrons and those of the conduction band.

The crystal structures of many of these Ce*TX* compounds can effectively be modified upon hydrogenation by filling tetrahedral voids. To give some examples, orthorhombic TiNiSi type CeRhGe transforms to hexagonal $CeRhGeH_2$[3] with a filled ZrBeSi type structure. Hydrogenation of CeRuGe with CeFeSi type leads to the filled version CeRuGeH[4] with ZrCuSiAs type. Furthermore, the La_2Sb type silicides and germanides *RE*ScSi and *RE*ScGe (*RE* = La, Ce) can be hydrogenated to *RE*ScSiH and *RE*ScGeH (*RE* = La, Ce)[5] with $SrZnBi_2$ type structure (filled La_2Sb variant). Only partial filling of the tetrahedral sites is observed for $CeRhSnH_{0.8}$ and $CeIrSnH_{0.7}$[6] with a ZrNiAl- and $CeRhSbH_{0.2}$[7] with a TiNiSi type metal substructure.

In all cases, the structural change is accompanied by drastic changes in the physical properties. For instance, hydrogen insertion leads to a transition from intermediate valence in CeNiIn to ferromagnetic ordering in $CeNiInH_{1.8}$,[8] or one can observe an increase of the Néel temperature (1.65 → 3.0 K) in the sequence CePdIn (Kondo antiferromagnet) → CePdInH.[9] In these systems, hydrogenation increases the unit cell volume and leads to a reduction in the coupling constant J_{cf} between the 4f(Ce) and conduction electrons. J_{cf} governs the competition between the indirect magnetic RKKY temperature T_{RKKY} proportional to J_{cf}^2 and the Kondo temperature T_K which exhibits an exponential dependence on J_{cf}. This competition is described by the Doniach phase diagram which shows that the reduction of J_{cf} favors Ce*TX*

Received: June 17, 2010
Revised: September 8, 2010
Published: January 21, 2011

ACS Publications © 2011 American Chemical Society

compounds strongly influenced by the Kondo effect, the occurrence or the increase of magnetic ordering for cerium.[9]

Recently, we have studied the tetrelides CeZnX (X = Ge, Sn, Pb)[10−12] with YPtAs[13] type structure, space group $P6_3/mmc$, a superstructure variant of AlB_2.[14] These structures are built up from puckered $[Zn_3X_3]^{\delta-}$ hexagons, which are separated and charge balanced by the cerium atoms. The $[Zn_3X_3]^{\delta-}$ hexagons show a stacking sequence $ABB'A'$. CeZnX (X = Ge, Sn, Pb) show stable trivalent cerium and magnetic ordering at low temperature at T_C = 4.6 (Ge) and 5.2 K (Sn), respectively T_N = 3.8 K (Pb). This leads to electron precise formulations $Ce^{3+}Zn^{2+}X^{4-}\cdot e^-$, leaving one surplus electron in metal centered bands, which account for the metallic conductivity of these materials.

The surplus electron is an excellent prerequisite for reduction of the CeZnX compounds upon hydrogenation. We have started hydrogenation experiments of CeZnSn and readily observed hydrogen incorporation. Herein we report on the structure, magnetic, and electric properties and chemical bonding of the new hydride $CeZnSnH_{1.5}$

EXPERIMENTAL AND THEORETICAL METHODOLOGY

Syntheses. Starting materials for the preparation of CeZnSn were a cerium ingot (Johnson-Matthey), zinc (Merck), and tin granules (Merck); all with stated purities better than 99.9%. The sample was synthesized by induction melting of the elements in a sealed tantalum ampule as described previously.[10] The purity of the CeZnSn precursor was checked by X-ray powder diffraction.

Hydrogen absorption experiments were performed using the apparatus described previously.[15] Small pieces of the annealed CeZnSn sample were heated under vacuum at 553 K for 4 h and then exposed to 4 MPa of hydrogen gas (99.999% as purity) at the same temperature for two days. The hydrogenation induces a decrepitation of the starting material. The amount of hydrogen absorbed was determined volumetrically by monitoring pressure changes in a calibrated volume. Under these conditions, the new hydride $CeZnSnH_{1.6(1)}$ was obtained. The latter is stable in ambient conditions.

X-ray Powder Diffraction. The hydride sample was characterized through a Guinier powder pattern (Cu Kα_1 radiation, α-quartz: a = 491.30 and c = 540.46 pm as internal standard). The Guinier camera was equipped with an imaging plate technique (Fujifilm, BAS-READER 1800). The hexagonal lattice parameters (Table 1) were obtained through a least-squares routine. The correct indexing was ensured through comparison of the experimental pattern with a calculated one.[16] The powder pattern of $CeZnSnH_{1.5}$ showed much weaker superstructure reflections than the initial stannide [10], e.g. 4.2 vs 13.9% for 013 and 2.0 vs 12.2% for 017. In agreement with the strong enlargement of the c-axis, this was already a hint for much weaker puckering of the Zn_3Sn_3 networks.

Single Crystal X-ray Data. Small irregularly shaped crystal fragments were isolated from the crushed hydrogenated $CeZnSnH_{1.5}$ sample and mounted on quartz fibers using bees wax. The crystals were investigated on a Buerger precession camera (white Mo radiation, Fujifilm imaging plate) in order to check the quality for intensity data collection. The data set was collected at room temperature by use of an IPDS II diffractometer (graphite monochromatized Mo Kα radiation; oscillation mode). A numerical absorption correction was applied to the data set. Details on the crystallographic data are given in Table 1.

Electron Diffraction. Electron diffraction experiments were performed with a JEOL 2000FX microscope equipped with a double tilt specimen holder. The microscope was used at an accelerating voltage of 200 kV. The powder was ground in ethanol and a droplet of this suspension was then deposited on a holey carbon grid. Electron diffraction experiments were carried out on many crystallites of the hydride and very reproducible results were observed.

Table 1. Crystal Data and Structure Refinement of $CeZnSnH_{1.5}$ (Space Group $P6_3/mmc$, Z = 4)

empirical formula	$CeZnSnH_{1.5}$
formula weight, gmol^{-1}	325.2
unit cell dimensions (Guinier data)	
a, pm	449.34(9)
c, pm	1731.3(4)
V, nm^3	0.3027
calculated density, g cm^{-3}	7.11
crystal size, μm^3	10 × 50 × 60
transm. ratio (max/min)	2.13
absorption coefficient, mm^{-1}	30.5
F(000), e	552
θ range for data collection, deg	2−31
range in hkl	±6; ±6; ±24
total no. reflections	2957
independent reflections/R_{int}	218/0.0473
reflections with $I \geq 2\sigma(I)/R\sigma$	157/0.0207
data/parameters	218/12
goodness-of-fit on F^2	1.093
final $R1/wR2$ indices [$I \geq 2\sigma(I)$]	0.0323/0.0434
final $R1/wR2$ indices (all data)	0.0623/0.0493
extinction coefficient	0.0015(3)
largest diff peak/hole, e Å^{-3}	1.56/−0.86

Physical Property Measurements. For physical properties measurements, the hydride $CeZnSnH_{1.5}$ was compacted at room temperature (compactness ≈80%) in order to form a polycrystalline pellet (diameter =6 mm and thickness =3 mm) and then heated for 2 days at 553 K under a pressure (4 MPa) of hydrogen. After this thermal treatment, which improved the mechanical behavior, the pellet was checked by X-ray diffraction; no structural change was evident. For electrical resistivity measurements, a bar of 1.5 × 1.5 × 5 mm^3 was cut from the pellet. The measurement was carried out above 4.2 K using the standard dc four probe method with silver paint contacts and an intensity current of 10 mA. *Due to the presence of microcracks in the pellet, the absolute value of $\rho(T)$ could not be determined accurately; for this reason, a reduced representation $\rho(T)/\rho(270\ K)$ is chosen.*

Magnetization measurements were performed on a part of the pellet using a Superconducting Quantum Interference Device (SQUID) magnetometer in the temperature range 1.8−300 K and applied fields up to 46 kG. Corrections for both diamagnetic and conduction electron contributions as well as demagnetization effects have not been applied.

Heat capacity measurements on the hydride $CeZnSnH_{1.5}$ were performed by a relaxation method with a Quantum Design PPMS system and using a two-tau model analysis. Data were taken in the 2−50 K temperature range. For these latter measurements, the sample was a plate of weight 27.3 mg obtained from the same pellet used for the other physical characterization.

A $Ca^{119m}SnO_3$ source was available for the ^{119}Sn investigations and a palladium foil of 0.05 mm thickness was used to reduce the tin K X-rays concurrently emitted by this source. The measurements were performed in the usual transmission geometry in commercial helium bath and flow cryostats. The temperature of the absorber could be varied from 4.2 to 300 K. The source was kept at room temperature in all experiments. The sample was placed within a thin-walled PVC container at a thickness corresponding to about 10 mg Sn/cm^2.

Computational Details. Two computational methods were used in the framework of density functional theory (DFT).[17] A pseudo potential approach within the Vienna ab initio simulation package (VASP)

Table 2. Atomic Coordinates and Anisotropic Displacement Parameters (pm^2) for $CeZnSnH_{1.5}$[a]

atom	wyck	x	y	z	$U_{11} = U_{22}$	U_{33}	U_{eq}
Ce1	2a	0	0	0	98(6)	100(5)	98(4)
Ce2	2b	0	0	1/4	105(6)	104(5)	105(4)
Zn	4f	1/3	2/3	0.1260(2)	107(5)	388(16)	201(6)
Sn	4f	1/3	2/3	0.6200(1)	75(3)	167(4)	105(3)

[a] U_{eq} is defined as one-third of the trace of the orthogonalized U_{ij} tensor. The anisotropic displacement factor exponent takes the following form: $-2\pi^2[(ha^*)2U_{11} + ... + 2hka^*b^*U_{12}]$. $U_{13} = U_{23} = 0$; $U_{12} = 1/2U_{11}$.

code[18] was first called for to optimize the hydrogen positions and to obtain the equation of states (EOS) for CeZnSn and its hydride as well as a charge density analysis with the Bader atoms in molecules and crystals approach.[19b] For this, we use projector augmented wave (PAW) potentials[20] which account for 4f(Ce) states, built within the generalized gradient approximation (GGA) scheme.[21] The calculations were converged at an energy cutoff of 300 eV for the plane-wave basis set with respect to the *k*-point integration with a starting mesh of 4 × 4 × 4 up to 8 × 8 × 8 for best convergence and relaxation to zero strains. The Brillouin-zone integrals were approximated using a special *k*-point sampling.

The all-electron calculations are based on the DFT and GGA functional.[21] They were performed using the full potential scalar-relativistic augmented spherical wave (ASW) method (see refs 22 and 23 and refs therein). In the ASW method, the wave function is expanded in atom-centered augmented spherical waves, which are Hankel functions and numerical solutions of Schrödinger's equation, respectively, outside and inside the so-called augmentation spheres. In the minimal ASW basis set, we chose the outermost shells to represent the valence states and the matrix elements were constructed using partial waves up to $l_{max} + 1 = 4$ for Ce, i.e., 4f(Ce) were considered within the basis set, $l_{max} + 1 = 3$ for Zn and Sn and finally $l_{max} + 1 = 2$ for H. Self-consistency was achieved by a highly efficient algorithm for convergence acceleration.[24] The Brillouin zone integrations were performed using the linear tetrahedron method with up to 1088 *k*-points within the irreducible wedge.[19b,23] The efficiency of this method in treating magnetism and chemical bonding properties in transition metal, lanthanide, and actinide compounds has been well demonstrated in recent years.[25,26]

The relative magnitude of the chemical bonding is obtained based on the overlap population analysis: S_{ij}, *i* and *j* being two chemical species. The crystal orbital overlap population (COOP) criterion is used.[27] For the purpose of establishing trends of chemical bonding strength, we show the integrated COOP (*i*COOP): the larger the area below the curves the larger the bonding is. In the plots positive, negative, and zero *i*COOP magnitudes indicate bonding, antibonding, and nonbonding interactions, respectively.

RESULTS AND DISCUSSION

Structural Refinement. Analyses of the diffractometer data set of a crystal from the hydrogenated sample revealed the pronounced AlB_2 subcell, but weaker reflections enforced a 4-fold cell along the *c*-axis, similar to the parent stannide.[10] The systematic extinctions led to space group $P6_3/mmc$. The atomic parameters of CeZnSn[10] were then taken as starting values and the structure was refined using SHELXL-97 (full-matrix least-squares on F^2)[28] with anisotropic atomic displacement parameters for all atoms. Refinement of the occupancy parameters showed full occupancy within two standard deviations. The final difference electron-density synthesis was flat. Determination of possible hydrogen sites was not possible on the basis of the present X-ray data. The results of the structure refinement are summarized in Table 1. The atomic coordinates and the interatomic distances are listed in Tables 2 and 3. Further information on the structure refinement is available from: Fachinformationszentrum Karlsruhe, D-76344 Eggenstein-Leopoldshafen (Germany), by quoting the Registry No. CSD-421872.

Table 3. Interatomic Distances (pm) Calculated with the Powder Lattice Parameters of CeZnSn and $CeZnSnH_{1.5}$[a]

			CeZnSn	$CeZnSnH_{1.5}$
Ce1	6	Sn	328.4	332.4
	6	Zn	368.3	338.9
	2	Ce2	418.5	432.8
	6	Ce1	456.7	449.3
Ce2	6	Zn	309.1	336.8
	6	Sn	345.2	343.4
	2	Ce1	418.5	432.8
	6	Ce2	456.7	449.3
Zn	3	Sn	270.8	259.6
	3	Ce2	309.1	336.8
	3	Ce1	322.6	338.9
Sn	3	Zn	270.8	259.6
	3	Ce1	328.4	332.4
	3	Ce2	345.2	343.4

[a] Standard deviations are all equal or smaller than 0.2 pm. All distances within the first coordination spheres are listed.

Electron Diffraction Studies. Electron diffraction data are fully consistent with the analysis of the X-ray diffraction data discussed above. The [100] zone axis pattern (Figure 1) obviously reveals the AlB_2 subcell (intense reflections) and a 4-fold superstructure along the c^* direction. The $[1\bar{1}0]$ zone axis pattern clearly shows the existence of the reflection condition: $hhl\ l = 2n$. This observation and the absence of reflection condition in the [100] zone axis pattern indicate that the extinction symbol corresponding to the material is *P--c* which is consistent with the proposed $P6_3/mmc$ space group. Note that, in the [100] zone axis pattern, all the reflections appear along c^* due to a double diffraction phenomenon.

A very careful observation of the patterns shows the presence of a hardly visible modulation around the main spots. This means that a long-range ordering exists in the material. Nevertheless, as it has not been observed during the X-ray diffraction experiments; its origin will remain unknown.

Crystal Chemistry. The new hydride $CeZnSnH_{1.5}$ is the first hydride of a ternary intermetallic compound with YPtAs type[13] structure. The cerium, zinc, and tin positions have unambiguously been determined and refined from single crystal diffractometer data and the unit cell of the hydride was confirmed by electron diffraction.

Hydrogenation has a drastic effect on the lattice parameters. The unit cell shows a small, but anisotropic expansion, i.e. 456.7 → 449.34 pm for the *a* and 1673.8 → 1731.3 pm for the *c* parameter. The strong increase of *c* along with the hydrogen insertion leads to a drastic flattening of the $[Zn_3Sn_3]$ networks (Figure 2) which now have pronounced two-dimensional character. All interlayer Zn−Zn, Zn−Sn, and Sn−Sn contacts can safely be considered as nonbonding. The anisotropic cell expansion leads to a drastic decrease of the Zn−Sn intralayer distance from 271 pm in CeZnSn to 260 pm in $CeZnSnH_{1.5}$. The latter are even shorter

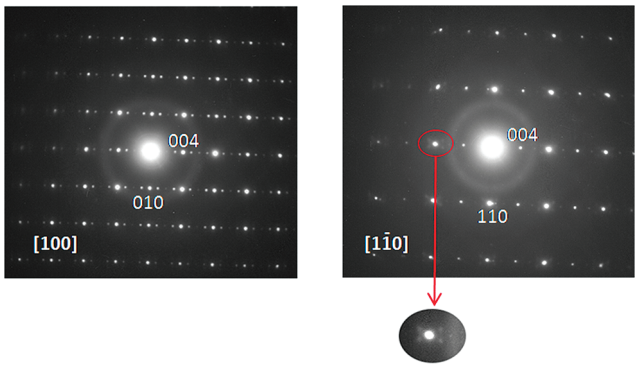

Figure 1. Electron diffraction patterns of $CeZnSnH_{1.5}$. The inset underlines the presence of very weak modulation reflections.

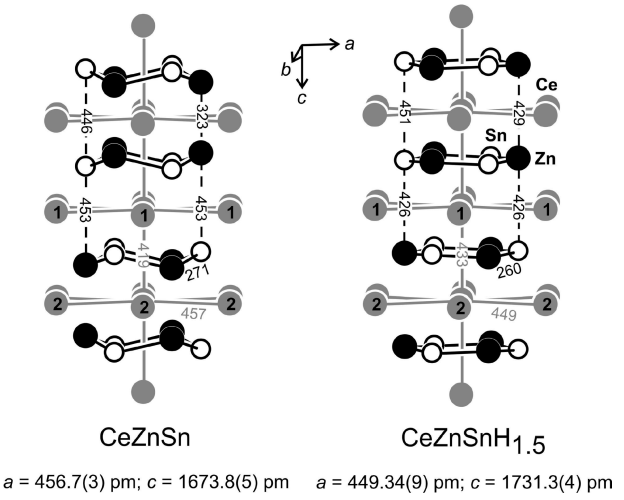

Figure 2. Cutout of the CeZnSn (YPtAs type) and $CeZnSnH_{1.5}$ type structures. Cerium, zinc, and tin atoms are drawn as light gray, black filled, and open circles, respectively. The puckered Zn_3Sn_3 hexagons in CeZnSn and the almost planar Zn_3Sn_3 hexagons in $CeZnSnH_{1.5}$, relevant interatomic distances, and the crystallographically independent cerium sites are indicated. The hydrogen sites could not be refined from the single crystal X-ray data.

than the sum of the covalent radii[29] of 265 pm, indicating substantial Zn−Sn bonding within the layers, i.e., an increased Zn−Sn bond strength in the hydride.

Similar geometrical behavior has been observed for the series CeRhGe → $CeRhGeH_{1.8}$ and CeIrGe → $CeIrGeH_{1.8}$.[3] The strongly puckered $[Rh_3Ge_3]$ and $[Ir_3Ge_3]$ networks in the orthorhombic TiNiSi type germanides become planar in the hexagonal ZrBeSi type hydrides $CeRhGeH_{1.8}$ and $CeIrGeH_{1.8}$.

Also the Ce−Ce distances are affected by the hydrogenation. The most pronounced change concerns the Ce1−Ce2 distance between the layers which increases from 419 (CeZnSn) to 433 pm ($CeZnSnH_{1.5}$), while the Ce1−Ce1 and Ce2−Ce2 distances within the layers (corresponding to the lattice parameter *a*) slightly decrease from 457 (CeZnSn) to 449 pm ($CeZnSnH_{1.5}$). Nevertheless, all Ce−Ce distances are well above the Hill limit[30] of 340 pm for 4f electron localization.

Since the crystal chemistry and chemical bonding of the ternary YPtAs related materials has already been discussed in detail,[10−13,31] herein we refer only to the crystal chemical peculiarities of the quaternary hydride. Similar to the hydrides $CeRhGeH_{1.8}$

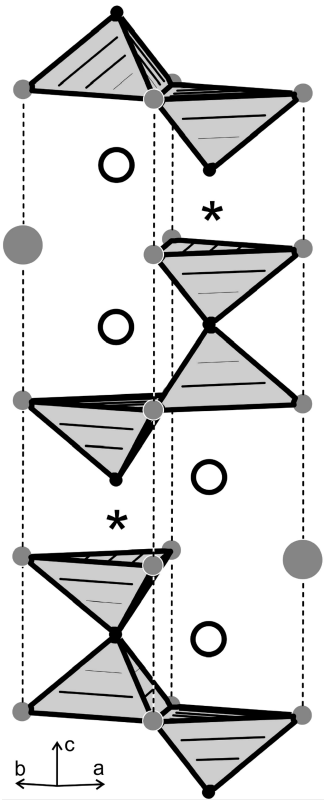

Figure 3. Noncentrosymmetric model (space group $P6_3mc$) for the hydrogen sites in $CeZnSnH_{1.5}$. Cerium, zinc, and tin atoms are drawn as light gray, black filled, and open circles, respectively. The hydrogen centered Ce_3Zn tetrahedra are emphasized. Asterisks mark tetrahedra that cannot be occupied for steric reasons.

and $CeIrGeH_{1.8}$,[3] also the hydrogen atoms in $CeZnSnH_{1.5}$ fill $ZnCe_3$ tetrahedral voids. Keeping the centrosymmetric model for the metal substructure of $CeZnSnH_{1.5}$ in mind, two crystallographically different voids can be filled. One type of them, however, concerns face-sharing tetrahedra and full hydrogen occupancy is not possible due to steric hindrance (much too short interatomic distances). Since only one of the face-sharing tetrahedral voids can be occupied, a noncentrosymmetric model in space group $P6_3mc$ (*translationengleiche* subgroup of $P6_3/mmc$) has been developed (Figure 3; empty tetrahedra are marked with asterisks). In that model, 1.5 hydrogen atoms per formula unit can be placed in $ZnCe_3$ tetrahedra, in good agreement with the volumetrically determined hydrogen amount. Filling of the remaining tetrahedral voids would only be possible by a drastic increase of the *c* parameter. This would significantly weaken the interlayer chemical bonding. The situation in these YPtAs related hydrides is thus different from the hydrides derived from the ZrNiAl type.[32−34] Since on the basis of X-ray diffraction it is not possible to locate hydrogen besides strongly scattering cerium, zinc, and tin, we refined the metal substructure with the centrosymmetric model.

Finally we turn back to the electron counting. The susceptibility measurements[11] clearly point to stable trivalent cerium in CeZnSn. Since the structure contains isolated tin atoms, an electron precise formulation $Ce^{3+}Zn^{2+}Sn4^{-}\cdot e^{-}$ results, which leaves one surplus electron in metal centered bands. Consequently only one hydrogen atom per formula unit would be sufficient for reduction. The stannide, however, incorporates 1.5 hydrogen

dx.doi.org/10.1021/cm1016504 |*Chem. Mater.* 2011, 23, 1096–1104

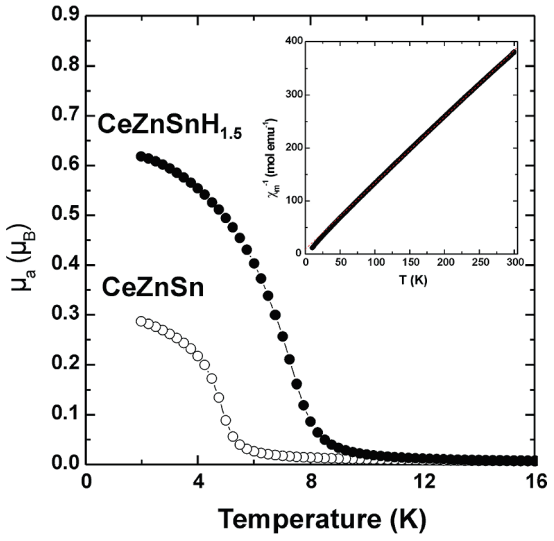

Figure 4. Temperature dependence of the magnetization M measured in an applied field of 1 kG for CeZnSn and its hydride. The inset shows the temperature dependence of the reciprocal magnetic susceptibility χ_m^{-1} for $CeZnSnH_{1.5}$.

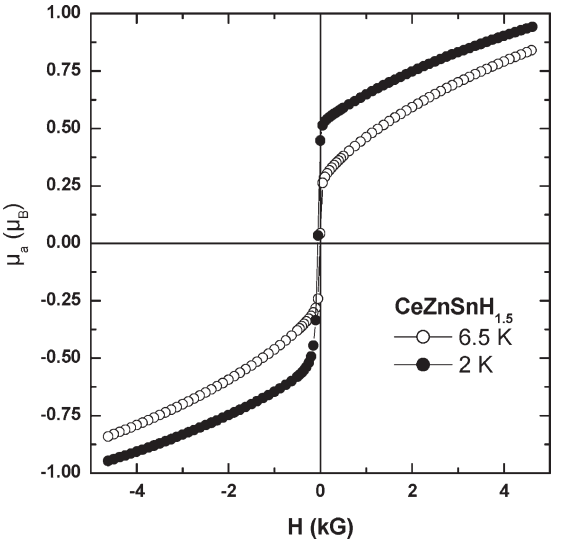

Figure 5. Field dependence at 2 and 6.5 K of the magnetization M of $CeZnSnH_{1.5}$.

atoms per formula unit. This circumstance is addressed in more detail below in Electronic Structure and Chemical Bonding Analyses.

Recently a number of structurally related quaternary hydrides $MAlSiH$ (M = Ca, Sr, Ba),[35] BaInGeH,[36] SrGaGeH, BaGaSiH, BaGaGeH, and BaGaSnH[37] have been reported. The triel and tetrel atoms form similar ordered $[Al_3Si_3]$, etc., networks, however, in a stacking sequence $A\,A$. In these hydrides, the hydrogen atoms bond to the triel atoms and the latter have distorted tetrahedral coordination. In contrast to metallic $CeZnSnH_{1.5}$, the alkaline earth metal based hydrides have electron precise compositions and are semiconducting, e.g. $Ba^{2+}Ga^{-}Ge^{0}H^{-}$.

Physical Properties. Figure 4 exhibits the variation of the atomic magnetic dipole moment μ_a vs T ($2 \le T \le 16$ K) for CeZnSn and its hydride. For both compounds, the strong increase of μ_a with increasing T characterizes the inset of ferromagnetic ordering. The Curie temperature T_C, determined from the inflection point of the $\mu_a = f(T)$ curve is 4.8 and 7.3 K for CeZnSn and its hydride, respectively. In other words, the hydrogenation induces an increase of the Curie temperature. A similar behavior was reported during the hydrogenation of the Kondo ferromagnet CePtAl.[38] Below T_C, the hysteresis curves for $CeZnSnH_{1.5}$ (Figure 5) agree with the behavior of a polycrystalline ferromagnet. The loops exhibit at 2 K a very small coercive field of 0.6 kG and $\mu_a = 0.42\ \mu_B$; μ_a is not saturated at 46 kG, reaching a value of 0.95 μ_B. This value of μ_a, notably smaller than that expected for a Ce^{3+} magnetic moment (2.14 μ_B /Ce), results from both the average powder of the sample and the influence of the crystal field effects as described previously for the hydride $CeNiSnH_{1.8}$.[39]

Figure 6 presents the paramagnetic region ($10 \le T \le 300$ K) of $CeZnSnH_{1.5}$ as variation μ_{eff} vs T[40] and, in the inset, as variation χ_m^{-1} vs T (CGS-emu units). The solid lines display the result of fitting procedures carried out with a model that considers spin−orbit coupling (H_{SO}), the crystal field (CF) effect (H_{CF}), exchange interactions between the cerium atoms (H_{ex}), and the influence of the applied magnetic field (H_{mag}; B = 30 kG).[41,42] H_{SO} splits the 14-fold degenerate $4f^1$ ground state into

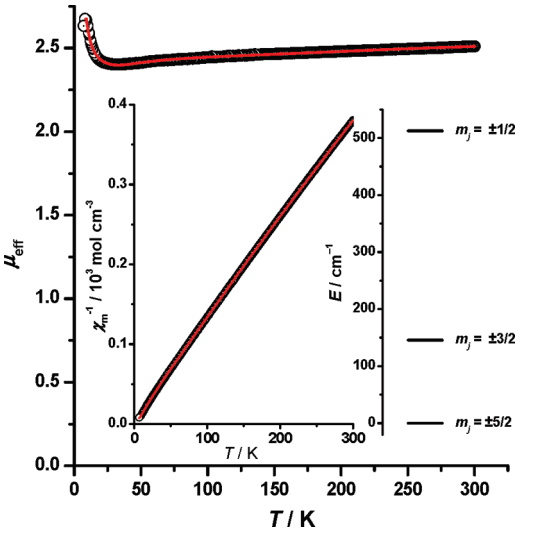

Figure 6. $CeZnSn_{1.5}$: Variation μ_{eff} vs T and χ_m^{-1} vs T (CGS-emu units). The solid lines result from fitting procedures to the experimental data on the basis of the model described in the text.

the ground multiplet $^2F_{5/2}$ and the excited multiplet $^2F_{7/2}$ where $\Delta E_{SO} \approx 2200$ cm^{-1}. With regard to H_{CF}, a model that reflects the individual CF parameters of the structurally different cerium atoms in the space group $P6_3/mmc$ (Ce1: point symmetry D_{3d}, six CF parameters. Ce2: D_{3h}, four CF parameters) is unfeasible on account of too many CF parameters. However, in $CeZnSnH_{1.5}$, the coordination polyhedra around both atoms Ce1 and Ce2 approximate a uniform polyhedron of pseudo symmetry D_{6h}, conditioned (i) by the flattening of the two-dimensional $[Zn_3Sn_3]$ networks—accompanied by a trend to unify corresponding intermetallic separations—and (ii) by similar electronegativities of Zn (1.6) and Sn (1.8) with the consequence that the CF contributions to H_{CF} are resembling.

The CF operator for D_{6h} symmetry, acting on the multiplets $^2F_{5/2}$ and $^2F_{7/2}$ of Ce^{III}, is composed of both CF parameters B_q^k and spherical tensors C_q^k, the latter related to the spherical

Table 4. $CeZnSnH_{1.5}$: Magnetically Relevant Parameters ζ_{4f}, B_q^k, λ_{mf}, and B for the paramagnetic region and CF splitting energies

parameters in cm^{-1}		CF splitting in $cm^{-1}/E(\pm m_J)$		
B/kG	30	$^2F_{5/2}$	$E(\pm 1/2)$	519
ζ_{4f}	625[a]		$E(\pm 3/2)$	150
B_0^2	929		$E(\pm 5/2)$	0
B_0^4	885			
λ_{mf}/mol cm^{-3}	5.55			
θ/K[b]	2.82			
SQ/%[c]	0.28			

[a] Free ion value. [b] Corresponding to a Curie−Weiss straight line in the temperature range 10−17 K. [c] Def.: SQ = $(FQ)^{1/2} \times 100$ where FQ = $\sum([X_{obs}(i) - X_{cal}(i)]X_{obs}i)^{1/2}$.

harmonics Y_q^k ($C_q^k = [4\pi/(2k+1)]^{1/2}Y_q^k$):[43,44]

$$\hat{H}_{CF}(D_{6h}) = B_0^2C_0^2 + B_0^4C_0^4 + B_0^6C_0^6 + B_6^6(C_6^6 + C_{-6}^6)$$

The Zeeman effect of the external magnetic field with flux density **B** in direction α is represented by $H_{mag,\alpha}$. To incorporate exchange interactions between the cerium atoms, the susceptibility equation is extended by the molecular field parameter λ_{mf}:

$$\hat{H}_{CF}(D_{\infty h}) = \chi_m^{-1}(\zeta, B_q^k, B) - \lambda_{mf}$$

where $\chi_m = (\chi_{m,\parallel} + 2\chi_{m,\perp})/3$; λ_{mf} produces a parallel shift of the χ_m^{-1} (ζ_{4f}, B_q^k, **B**)--T curve.[42] Fitting procedures proved that the axial CF parameters B_0^2 and B_0^4 are the dominating ones, and finally, it turned out that the CF effect is adaquately described by

$$\hat{H}_{CF}(D_{\infty h}) = B_0^2C_0^2 + B_0^4C_0^4$$

acting solely on the $^2F_{5/2}$ basis functions (goodness of the fit: $SQ = 0.3\%$; see footnote c in Table 4). Regarding the influence of the hydride ions within the $ZnCe_3$ voids, the energetic order of the three doublets $|\pm m_J\rangle$ (where $m_J = 1/2, 3/2, 5/2$), resulting from the $^2F_{5/2}$ ground multiplet under the action of $\hat{H}_{CF}$ ($D_{\infty h}$), is of interest (cf. Table 4 and Figure 6). The doublet $|\pm 5/2\rangle$ is the ground state, followed by $|\pm 3/2\rangle$ at 150 cm^{-1} and $|\pm 1/2\rangle$ at 519 cm^{-1}. This energy sequence of doublets is explainable by negatively charged ions arranged on the main axis with a short distance to the cerium atoms, that is, by the hydride ions occupying the tetrahedral holes of the $CeZn_3$ units: The 4f functions $|\pm 1/2\rangle$ of cerium are highest in energy because they have maxima of electron density in direction of the main axis, while corresponding maxima for $|\pm 5/2\rangle$ are in the plane perpendicular to the main axis and for $|\pm 3/2\rangle$ between both orientations (refs 42 page 304 and 45).

Inspection of the variation χ_m^{-1} vs T revealed Curie−Weiss behavior in the temperature range $10 \le T \le 17$ K with $\mu_{eff} = 2.23$ and $\theta = +2.8$ K, confirming the ground state $|\pm 5/2\rangle$ as well as the ferromagnetic behavior at lower temperature.

The temperature dependence of the reduced resistivity $\rho(T)/\rho(270\ K)$ of the hydride $CeZnSnH_{1.5}$ reveals several characteristics (Figure 7): (i) A downward curvature around 100−150 K. Such behavior, which is similar with that reported previously for CeNiSnH,[46] is expected for Kondo-type interactions in the presence of crystal field effects.[47] (ii) A small decrease around 12−8 K and then a higher decrease below 8−7 K (inset of Figure 7). This behavior of $\rho(T)/\rho(270\ K)$ below this last temperature range could be associated with the loss of spin disorder scattering of the conduction electrons owing to the occurrence of a ferromagnetic transition.

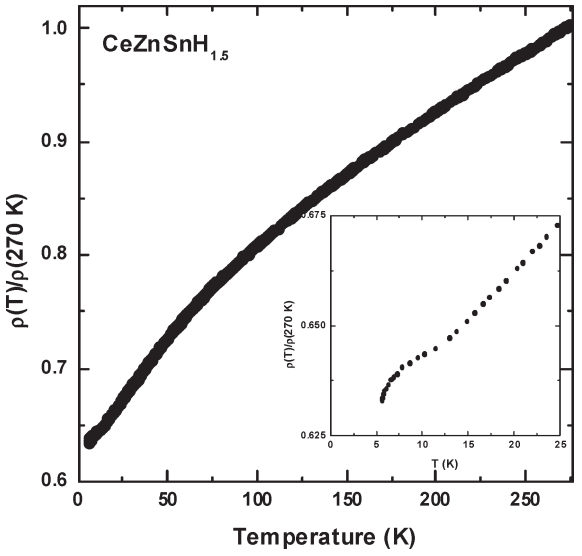

Figure 7. Temperature dependence of the reduced electrical resistivity $\rho(T)/\rho(270\ K)$ for $CeZnSnH_{1.5}$. The inset presents the low temperature part of this dependence.

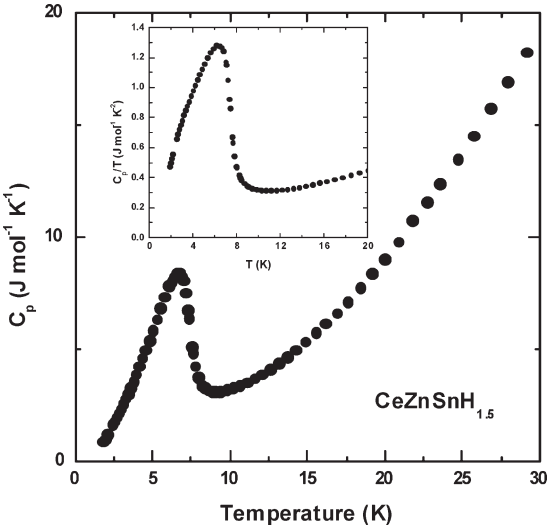

Figure 8. Temperature dependence of the specific heat C_p for $CeZnSnH_{1.5}$. The inset presents the C_p/T versus T curve.

The specific heat C_p of $CeZnSnH_{1.5}$ has been measured at zero magnetic field between 1.8 and 30 K. As presented in Figure 8, the temperature dependence of C_p divided by temperature exhibits a peak at about 6.8(2) K. This temperature agrees with the Curie temperature reported above by magnetization measurements (Figure 4) and confirms the ferromagnetic behavior of the hydride. Valuable information can be obtained from the entropy associated with the ferromagnetic ordering, which is estimated from the magnetic contribution to the specific heat in the low-temperature range as $C_{pmag} = C_p - (\gamma T + \beta T^3)$. Between 13 and 23 K, the fitting of $C_p/T = \gamma T + \beta T^2$ (inset of Figure 8) yields to an electronic coefficient γ = 237 mJ mol^{-1} K^{-2} and a phonon constant $\beta = 5.4 \times 10^{-4}$ J mol^{-1} K^{-4}. At T_C, the magnetic entropy reaches S_m = 5.372 J/(mol K) or 0.93 R ln 2, which is

dx.doi.org/10.1021/cm1016504 |*Chem. Mater.* 2011, 23, 1096–1104

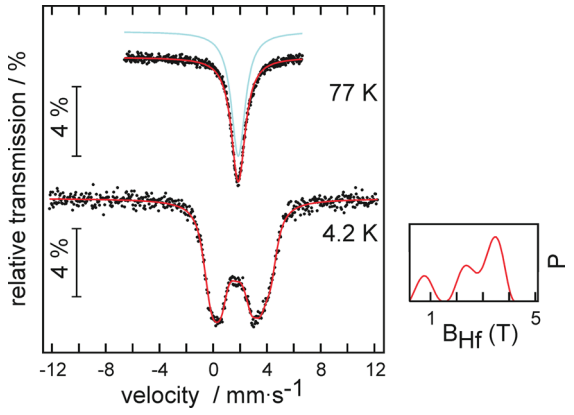

Figure 9. Experimental and simulated ^{119}Sn Mössbauer spectra of $CeZnSnH_{1.5}$ at 77 and 4.2 K. The temperature evolution of the field distribution functions, $P(B_{hf})$, obtained from computer fits of the 4.2 K data is presented at the right-hand part of the spectra.

Table 5. Fitting Parameters of ^{119}Sn Mössbauer Spectroscopic Measurements of $CeZnSnH_{1.5}$[a]

T (K)	δ (mm s^{-1})	Γ (mm s^{-1})	ΔE_Q (mm s^{-1})	B_{hf} (T)
77	1.87(1)	1.22(2)	0.17(6)	
4.2	2.17(3)	1.00*	0.26(2)	2.7

[a] Numbers in parentheses represent the statistical errors in the last digit: (δ), isomer shift; (Γ), experimental line width, (ΔE_Q), electric quadrupole interaction; B_{hf}, averaged magnetic hyperfine field. Values marked with an asterisk were kept fixed during the fitting procedure.

close to R ln 2 = 5.76 J mol^{-1} K^{-1}, the value expected for a doublet ground state of Ce^{3+}. This result suggests the small influence of the Kondo effect on the physical properties of the hydride $CeZnSnH_{1.5}$.

^{119}Sn Mössbauer Spectroscopy. The ^{119}Sn Mössbauer spectra of the $CeZnSnH_{1.5}$ sample were recorded at 77 and 4.2 K, well above and slightly below the Curie temperature. The spectra are presented in Figure 9 together with transmission integral fits. The corresponding fitting parameters are listed in Table 5. An electric quadrupole interaction of ΔE_Q = 0.17(6) respectively 0.26(2) mm/s observed at 77 respectively 4.2 K is caused by the noncubic local symmetry at the tin sites. The isomer shift of δ = 1.87(1) mm/s indicates a slightly lower electron density at the tin nucleus as expected because of the additional electron of the inserted hydrogen compared to the value for the non-hydrogenated compound CeZnSn (1.967(4) mm/s). These parameters compare well with the recently reported data for CeZnSn[10] and other equiatomic stannides such as PrRhSn[48] and HoRhSn.[49]

As illustrated in Figure 9, the low temperature spectrum has a more complicated shape due to magnetic splitting of the main doublet. However, the spectra could be effectively fitted assuming a distribution of hyperfine magnetic fields (multicomponent analysis), an approach similar to the Wivel and Mørup method.[50] The probability distribution curve $P(B_{hf})$ as a function of temperature is shown in Figure 9 beside the spectrum of 4.2 K. The averaged transferred hyperfine field is about 2.7 T, much larger than the one determined for CeZnSn (0.87 T).[10] A reason for the distribution of the hyperfine field is that the hydrogen content may not be exactly the same in all regions which leads to different domains having a slightly different electronic situation.

Table 6. Initially Calculated (from the $P6_3/mmc$ Model) Positions (with z_{calc}) for the Ordered $P6_3mc$ Model and Theoretically Calculated ones with z_{theo}[a]

atom	wyck	x	y	z_{calc}	z_{theo}
Ce1	2*a*	0	0	0	0
Ce2	2*a*	0	0	1/4	1/4
Zn1	2*b*	1/3	2/3	0.1262	0.118
Zn2	2*b*	1/3	2/3	0.3738	0.383
Sn1	2*b*	1/3	2/3	0.6198	0.636
Sn2	2*b*	1/3	2/3	0.8802	0.860
H1	2*b*	1/3	2/3	0.0150	0.011
H2	2*b*	1/3	2/3	0.2340	0.245
H3	2*b*	1/3	2/3	0.4850	0.484

[a] For details, see the text.

ELECTRONIC STRUCTURE AND CHEMICAL BONDING ANALYSES

Geometry Optimization and Equation of State. The hydrogen uptake within CeZnSn, resulting in the hydride causes a large increase of the *c* unit cell parameter and a slight contraction of the *a* parameter. From Figure 3 filling all the tetrahedral sites would result in too short H−H distances so that a model in the noncentrosymmetric space group $P6_3mc$ is used, where hydrogen atoms can be inserted to provide the experimental composition $CeZnSnH_{1.5}$ and reasonable H−H distances.

Full geometry optimization provides a calculated volume of 0.306 nm^3, in fair agreement with the experiment (0.3027 nm^3); the difference being expected within the approximations of the computational methodology. Regarding the hydrogen positions, the steric-based positioning of the atoms is confirmed from the calculations as it can be observed in Table 6 with only small deviations between the initial and final z coordinates. Nevertheless we have tested the hypothesis of positioning hydrogen within Ce_3Sn tertrahedra versus the choice of Ce_3Zn. For the purpose of establishing energy trends, the equation of state (EOS) is needed. This is because the calculated total energy pertains to the cohesive energy within the crystal, since the solution of the Kohn−Sham equations yield the energy with respect to infinitely separated electrons and nuclei. In as far as the zero of energy depends on the choice of the pseudopotentials, somehow it becomes arbitrary; i.e. it is shifted, not scaled. However, the energy derivatives as well as the equations of state remain unaltered. For this reason, one needs to establish the EOS and extract the fit parameters for an assessment of the equilibrium values. The energy versus volume, $E(V)$, curves are plotted around the experimental volume. In general they present a quadratic variation and they can be fitted with a Birch EOS to the third-order:

$$E(V) = E_0(V_0) + \frac{9}{8} V_0 B \left[\left(\frac{V_0}{V} \right)^{2/3} - 1 \right]^2 + \frac{9}{16} B(B' - 4) V_0 \left[\left(\frac{V_0}{V} \right)^{2/3} - 1 \right]^3$$

where E_0, V_0, B_0, and B' are the equilibrium energy, the volume, the bulk modulus, and its pressure derivative, respectively. The corresponding curves for the two hydrogen positions within CeZnSn are given in Figure 10. The hydride system is found

dx.doi.org/10.1021/cm1016504 |*Chem. Mater.* 2011, 23, 1096–1104

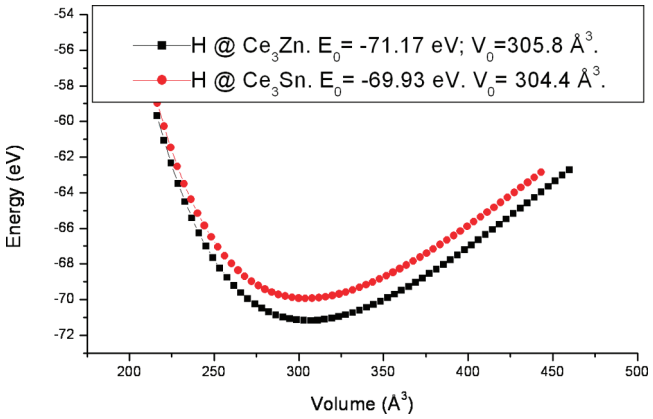

Figure 10. Equation-of-state: Energy versus volume in the nonmagnetic regime for CeZnSn hydride in two hypotheses.

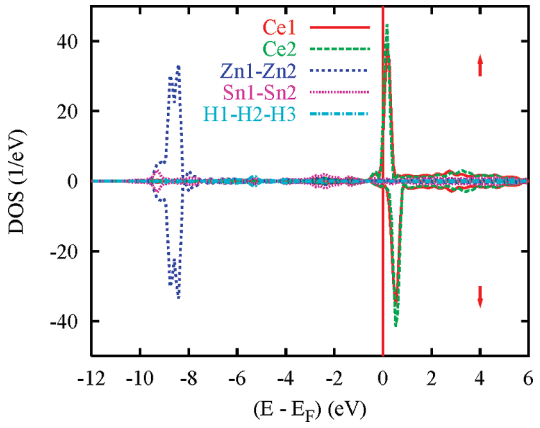

Figure 11. Site and spin projected density of states for $CeZnSnH_{1.5}$ regrouping Zn, Sn, and H curves.

stabilized when H atoms are positioned with Ce_3Zn tetrahedra, i.e., versus the hypothesis of Ce_3Sn, by 1.24 eV with a better agreement with experiment for the volume. The magnitudes of B_0 are 63 and 74 GPa for CeZnSn and $CeZnSnH_{1.5}$, respectively. They are within range of other Ce intermetallics[51] but the larger magnitude observed for the hydride is likely due to a hardening of the system due to metal−hydrogen bonding, mainly of Zn and Sn with H. B' values are close to 4, a value usually encountered in EOS computations.[51]

With respect to CeZnSn calculated in the same conditions, we get $E_0 = -49.67$ eV. Then for hypothesis H@Ce_3Zn (Figure 10), ΔE [$CeZnSnH_{1.5}$ − CeZnSn] = −21.5 eV for 4 formula units (fu), i.e. −5.375 eV for 1 fu $CeZnSnH_{1.5}$. Then the stabilization energy of H within CeZnSn is obtained from subtracting the energy per H taken alone:

$E_H = E(CeZnSnH_{1.5}) - E(CeZnSn) - 3/4E(H_2)$. $E(H_2)$ is the energy of the hydrogen molecule which is computed by considering a cubic super cell; its value is −6.5 eV. The obtained E_H magnitude is then −0.5 eV. This value is of smaller magnitude than in NdCoSiH where it amounts to −0.92 eV.[52] For assessing this result, we analyze the charge density output with the Bader "atoms in molecules and crystal concept".[19b] The result is that H does not fully ionize with H1, H2, and H3 charges amounting to −0.50, −0.57, and −0.50, respectively. This average value of $H^{-0.5}$ clearly indicates covalently bonded hydrogen in the intermetallic matrix. Note that the Bader analysis of MgH_2 calculated with the same method, gives Mg^{2+} and H^{-1}, i.e., an ionic hydride. This could explain why the hydrogen uptake with CeZnSn can be larger than 1.

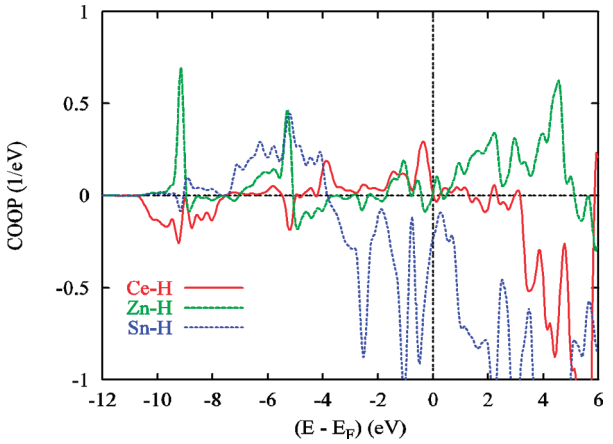

Figure 12. Crystal orbital overlap population plot for $CeZnSnH_{1.5}$.

All-Electron Calculations. Scalar relativistic spin only ASW calculations with the GGA functional show a magnetic polarization on both Ce sites with negligible magnetic moments on Zn and Sn. With respect to a spin degenerate configuration there is an energy gain of ∼3 eV per fu leading to confirm a magnetic ground state for $CeZnSnH_{1.5}$.

With magnitudes of $M(Ce1) = 0.57\,\mu_B$ and $M(Ce2) = 0.66\,\mu_B$, there is a lowering of the magnetic moments on Ce with respect to pristine CeZnSn where we computed magnetic moments carried by Ce as the following: $M(Ce1) = 0.831\,\mu_B$ and $M(Ce2) = 0.889\,\mu_B$.[10] This is likely due to the bonding between Ce and H whereby less electrons are magnetically polarized (cf. next paragraphs).

The spin and site projected density of states (PDOS) are shown in Figure 11. Low energy lying Sn $4d^{10}$ were considered as core states while Zn $3d^{10}$ were part of the valence basis set just like the 4f(Ce) states. At the lower part of the valence band, the Sn $3d^{10}$ PDOS is observed and the s, p states are smeared out with a PDOS running from −8 eV up to E_F for Zn and Sn as well as the itinerant part of Ce. The major part of the 4f(Ce) PDOS are centered above E_F due to the low filling of the cerium 4f subshell. The energy shift between the cerium spin-up (↑) and spin-down (↓) PDOS causes the occurrence of the magnetic polarization. We observe almost the same for the two Ce substructures (close magnitudes of the magnetic moments).

The chemical bonding peculiarities obtained from the COOP are shown in Figure 12. As expected from the hydrogen coordination polyhedra and from distance criteria (long Ce−H distances d(Ce−H) = 0.26 nm vs shorter d(Zn−H) = 0.19 nm) and due to the s, p character of Zn and Sn, stronger bonding is found especially at the lower part of the valence. Where Zn(Sn)−H bonding shows at the lower part of the VB, Ce−H interaction is antibonding. This is followed by Sn−H antibonding COOP for in the middle of the VB due to the involvement of Sn−p state with metal−metal bonding of the intermetallic, then below E_F there can be observed bonding Ce−H COOP's. Interestingly they occur at the location of 4f(Ce) states whence the lowering of the moment on Ce sites in the hydride.

dx.doi.org/10.1021/cm1016504 |*Chem. Mater.* 2011, 23, 1096–1104

CONCLUSIONS

$CeZnSnH_{1.5}$ is the first hydride of an YPtAs-type host compound. $CeZnSnH_{1.5}$ was obtained through hydrogenation of CeZnSn at 553 K and 4 MPa H_2 pressure. The hydrogen atoms fill three crystallographically independent $ZnCe_3$ tetrahedral sites. Hydrogenation anisotropically expands the unit cell parameters, i.e., −1.6% for *a* and +3.4% for *c*, leading to a flattening of the [ZnSn] layers. Hydrogenation strongly influences the hybridization of the cerium atoms and one observes an increase of the Curie temperature from 4.8 K for CeZnSn to 7.3 K for $CeZnSnH_{1.5}$. Electronic structure calculations reveal that filling of the $ZnCe_3$ tetrahedra is energetically more stable than filling of the $SnCe_3$ tetrahedra.

AUTHOR INFORMATION

Corresponding Author

*E-mail: pottgen@uni-muenster.de, chevalie@icmcb-bordeaux.cnrs.fr.

ACKNOWLEDGMENT

This work was financially supported by the Deutsche Forschungsgemeinschaft. W.H. is indebted to the Fonds der Chemischen Industrie and the NRW Graduate School of Chemistry for a Ph.D. stipend. We acknowledge computational facilities provided by the University Bordeaux 1 on the MCIA-M3PEC supercomputers.

REFERENCES

(1) Szytuła, A.; Leciejewicz, J. *Handbook of Crystal Structures and Magnetic Properties of Rare Earth Intermetallics*; CRC Press: Boca Raton, FL, 1994.
(2) Kraft, R.; Pöttgen, R.; Kaczorowski, D. *Chem. Mater.* **2003**, *15*, 2998.
(3) Chevalier, B.; Gaudin, E.; Al Alam, A. F.; Matar, S. F.; Weill, F.; Heying, B.; Pöttgen, R. *Z. Naturforsch.* **2008**, *63b*, 685.
(4) Chevalier, B.; Gaudin, E.; Geibel, C.; Canales, N. C.; Hermes, W.; Pöttgen, R. *J. Phys.: Condens. Matter* **2010**, *22*, 046003.
(5) Chevalier, B.; Hermes, W.; Heying, B.; Rodewald, U. Ch.; Hammerschmidt, A.; Matar, S. F.; Weill, F.; Pöttgen, R. *Chem. Mater.* **2010**, *22*, 5013.
(6) Chevalier, B.; Sebastian, C. P.; Pöttgen, R. *Solid State Sci.* **2006**, *8*, 1000.
(7) Chevalier, B.; Decourt, R.; Heying, B.; Schappacher, F. M.; Rodewald, U. Ch.; Hoffmann, R.-D.; Pöttgen, R.; Eger, R.; Simon, A. *Chem. Mater.* **2007**, *19*, 28.
(8) Chevalier, B.; Kahn, M. L.; Bobet, J.-L.; Pasturel, M.; Etourneau, J. *J. Phys.: Condens. Matter* **2002**, *14*, L365.
(9) Chevalier, B.; Wattiaux, A.; Bobet, J.-L. *J. Phys.: Condens. Matter* **2006**, *18*, 1743.
(10) Hermes, W.; Matar, S. F.; Harmening, T.; Rodewald, U.Ch.; Eul, M.; Pöttgen, R. *Z. Naturforsch.* **2009**, *64b*, 175.
(11) Hermes, W.; Pöttgen, R. *Z. Naturforsch.* **2009**, *64b*, 361.
(12) Hermes, W.; Rodewald, U. Ch.; Chevalier, B.; Matar, S. F.; Eyert, V.; Pöttgen, R. *Solid State Sci.* **2010**, *12*, 929.
(13) Wenski, G.; Mewis, A. *Z. Kristallogr.* **1986**, *176*, 125.
(14) Hoffmann, R.-D.; Pöttgen, R. *Z. Kristallogr.* **2001**, *216*, 127.
(15) Bobet, J.-L.; Pechev, S.; Chevalier, B.; Darriet, B. *J. Alloys Compd.* **1998**, *267*, 136.
(16) Yvon, K.; Jeitschko, W.; Parthé, E. *J. Appl. Crystallogr.* **1977**, *10*, 73.
(17) Hohenberg, P.; Kohn, W. *Phys. Rev.* **1964**, *136*, B864. Kohn, W.; Sham, L. J. *Phys. Rev.* **1965**, *140*, A1133.
(18) Kresse, G.; Furthmüller, J. *Phys. Rev. B* **1996**, *54*, 11169.
(19) (a) Tang, W.; Sanville, E.; Henkelman, G. *J. Phys.: Condens. Matter* **2009**, *21*, 84204.(b) http://www.chemistry.mcmaster.ca/aim/aim_0.html.
(20) (a) Blöchl, P. E. *Phys. Rev. B* **1994**, *50*, 17953. (b) Kresse, G.; Joubert, J. *Phys. Rev.* **1999**, *B59*, 1758.
(21) Perdew, J. P.; Burke, K.; Ernzerhof, M. *Phys. Rev. Lett.* **1996**, *77*, 3865.
(22) Williams, A. R.; Kübler, J.; Gelatt, C. D. *Phys. Rev. B* **1979**, *19*, 6094.
(23) Eyert, V. The Augmented Spherical Wave Method - A Comprehensive Treatment. *Lecture Notes in Physics*; Springer: Berlin Heidelberg, 2007, p 719.
(24) Eyert, V. *J. Comput. Phys.* **1996**, *124*, 271.
(25) Matar, S. F.; Riecken, J. F.; Chevalier, B.; Pöttgen, R.; Al Alam, A. F.; Eyert, V. *Phys. Rev. B* **2007**, *76*, 174434.
(26) Matar, S. F.; Gaudin, E.; Chevalier, B.; Pöttgen, P. *Solid State Sci.* **2007**, *9*, 274.
(27) Hoffmann, R. *Angew. Chem., Int. Ed. Engl.* **1987**, *26*, 846.
(28) Sheldrick, G. M., *SHELXL-97*, Program for Crystal Structure Refinement; University of Göttingen, Germany, 1997.
(29) Emsley, J. *The Elements*; Clarendon Press: Oxford, 1989.
(30) Hill, H. H. In *Plutonium and other Actinides*; Nuclear Materials Series; Mines, W. N., Ed.; AIME: 1970; Vol. 17, p 2.
(31) Gibson, B. J.; Kremer, R. K.; Jepsen, O.; Garrett, J. D.; Hoffmann, R.-D.; Pöttgen, R. *J. Phys. C* **2001**, *13*, 3123.
(32) Ravindran, P.; Vajeeston, P.; Vidya, R.; Kjekshus, A.; Fjellvåg, H. *Phys. Rev. Lett.* **2002**, *89*, 106403.
(33) Yartys, V. A.; Denys, R. V.; Hauback, B. C.; Fjellvåg, H.; Bulyk, I. I.; Riabov, A. B.; Kalychak, Ya. M. *J. Alloys Compd.* **2002**, *330−332*, 132.
(34) Vajeeston, P.; Ravindran, P.; Vidya, R.; Kjekshus, A.; Fjellvåg, H.; Yartys, V. A. *Phys. Rev. B* **2003**, *67*, 014101.
(35) Lee, M. H.; Björling, T.; Hauback, B. C.; Utsumi, T.; Moser, D.; Bull, D.; Noréus, D.; Sankey, O. F.; Häussermann, U. *Phys. Rev. B* **2008**, *78*, 195209.
(36) Evans, M. J.; Kranak, V. F.; Garcia-Garcia, F. J.; Holland, G. P.; Daemen, L. L.; Proffen, T.; Lee, M. H.; Sankey, O. F.; Häussermann, U. *Inorg. Chem.* **2009**, *48*, 5602.
(37) Evans, M. J.; Lee, M. H.; Holland, G. P.; Daemen, L. L.; Sankey, O. F.; Häussermann, U. *J. Solid State Chem.* **2009**, *182*, 2068.
(38) Bobet, J.-L.; Chevalier, B.; Weill, F.; Etourneau, J. *J. Alloys Compd.* **2002**, *330−332*, 373.
(39) Chevalier, B.; Bobet, J.-L.; Pasturel, M.; Bauer, E.; Weill, F.; Decourt, R.; Etourneau, J. *Chem. Mater.* **2003**, *15*, 2181.
(40) Definition: $\mu_{eff} = 2.83(\chi_m T)^{1/2}$ (CGS-emu units).
(41) Schilder, H.; Lueken, H. *J. Magn. Magn. Mater.* **2004**, *281*, 17.
(42) Lueken, H. *Magnetochemie*; Teubner: Stuttgart, 1999.
(43) Wybourne, B. G. *Spectroscopic Properties of Rare Earths*; Wiley: New York, London, Sydney, 1965.
(44) Görller-Walrand, C.; Binnemans, K. Rationalization of crystal-field parametrization. In *Handbook on the Physics and Chemistry of Rare Earths*; Gschneidner, K. A., Jr., Eyring, L., Eds.; Elsevier: Amsterdam, 1996; Vol. 23, Chapter 155, p 121.
(45) (a) Lueken, H.; Meier, M.; Klessen, G.; Bronger, W.; Fleischhauer, J. *J. Less-Common Met.* **1979**, *63*, P35. (b) Schröder, A.; van den Berg, R.; v. Löhneysen, H.; Paul, W.; Lueken, H. *Solid State Commun.* **1988**, *65*, 99.
(46) Chevalier, B.; Pasturel, M.; Bobet, J.-L.; Etourneau, J.; Isnard, O.; Sanchez Marcos, J.; Rodriguez Fernandez, J. *J. Magn. Magn. Mater.* **2004**, *272−276*, 576.
(47) Cornut, B.; Coqblin, B. *Phys. Rev. B* **1972**, *5*, 4541.
(48) Łątka, K.; Kmiec, R.; Gurgul, J.; Rams, M.; Pacyna, A. W.; Schmidt, T.; Pöttgen, R. *J. Solid State Chem.* **2005**, *178*, 3101.
(49) Gurgul, J.; Łątka, K.; Pacyna, A. W.; Sebastian, C. P.; Pöttgen, R. *Intermetallics* **2010**, *18*, 129.
(50) Wivel, C.; Mørup, S. *J. Phys. E* **1981**, *14*, 605.
(51) Matar, S. F. *Prog. Solid State Chem.* **2010**, *38*, 1.
(52) Tencé, S.; Matar, S. F.; André, G.; Gaudin, E.; Chevalier, B. *Inorg. Chem.* **2010**, *49*, 4836.